PII: S 0 9 5 5 - 7 9 9 7 (9 7) 0 0 0 8 1 - 7

ELSEVIER

A BEM formulation for anisotropic half-plane problems

Ernian Pan*, Chao-Shi Chen & Bernard Amadei

Department of Civil Engineering, University of Colorado, Boulder, CO 80309, USA

This article presents a boundary element formulation for cracked anisotropic elastic half-planes and shows how the formulation can efficiently be applied to solve various practical problems. The complete Green's functions for the anisotropic half-plane are obtained and the corresponding boundary integral equations are derived. Also presented are particular solutions associated with the body force of gravity and far-field stresses, which are incorporated rigorously into the boundary element formulation by superposition. For half-plane problems, this new formulation is more efficient than the finite element method or even the boundary element formulation using Green's functions for the infinite plane.

Numerical examples are presented for the calculation of the stresses and the stress intensity factors. For the isotropic case, our numerical results are in excellent agreement with those obtained with previously published analytical solutions. For the anisotropic case, our results show clearly that material anisotropy can have a great effect on the stress distribution and on the magnitude of stress intensity factors. © 1998 Elsevier Science Ltd.

Keywords: Boundary-element method, dual BEM, half-plane Green's functions, anisotropic elasticity, body force of gravity, fracture mechanics.

1 INTRODUCTION

Many problems in engineering and geosciences require models associated with a half-plane domain. Examples can be found in foundation engineering related to underground or surface excavations, in geophysics when estimating analytically the regional *in-situ* stresses in the Earth, and in advanced material science when studying the stability of rough surfaces or the initiation and propagation of flaws in heteroepitaxial thin films.

Previously, several analytical and numerical methods were proposed for the study of half-plane related problems. The first analytical method, called the bipolar coordinates transformation method, was used by Mindlin[1,2] and Ling[3] to study the behavior of a single circular opening in an isotropic half-plane. The perturbation method is another analytical approach which, under the assumption of small perturbation over a flat surface, can be suitable for studying topographically or morphologically induced stresses.[4–7]

*Department of Civil Engineering, University of Colorado, Boulder, CO 80309, USA.

The third analytical method is the exact conformal mapping method which can be successfully applied to half-plane geometries for which the exact conformal mapping function can be found;[8,9] Otherwise, the numerical conformal mapping technique can be applied.[10,11] However, for very complex geometries and boundary conditions, one needs to resort to numerical methods. Examples of application of the FEM to half-plane problems can be found in Zienkiewicz et al.,[12] Barla,[13] and Soliman et al.[14] An alternative to the FEM is the boundary element method (BEM) which, compared with the domain methods, requires discretization of the problem boundary only. Applications of BEM related methods to some specific half-plane problems were conducted previously by Eissa,[15] Fainstein et al.,[16] Carter and Alehossein,[17] Xiao and Carter[18] and Beer and Poulsen.[19] However, these researchers used Kelvin-type Green's functions in their formulation, which requires either discretization or approximation along the flat surface of the half-plane. The complete Green's functions in an isotropic half-plane were derived and used by

Tells and Brebbia[20] and Meek and Dai[21] in their BEM formulation. Green's functions and boundary integral equations were derived by Dumir and Mehta[22] for orthotropic half-plane problems. However, so far to the author's knowledge, there is no BEM formulation that can address generalized anisotropic half-plane problems.

The purpose of this article is to present such a BEM formulation. The complete Green's functions in the generalized anisotropic half-plane are derived and incorporated into the boundary integral equations so that the discretization along the horizontal flat surface can be avoided. Particular solutions corresponding to the body force of gravity and far-field stresses are also derived and included rigorously in the BEM formulation, which makes the problem very similar to the one associated with the homogeneous equations except that, for the body force and/or far-field stress cases, two extra integral terms related to the particular solutions are added to the integral equations. Therefore, for the far-field stress problem, for example, the artificial truncation of the semi-infinite domain, or the transferring of the far-field stress onto the boundary (or opening) of the problem is avoided.

In order to calculate the stress intensity factor (SIF) for cracked anisotropic half-planes, the formulation proposed recently by Pan and Amadei[23] is adopted and modified to include the body force of gravity and far-field stresses. In this BEM formulation, the displacement integral equation is collocated on the no-cracked boundary of the problem and the traction integral equation on one side of the crack surfaces.

Numerical examples are presented for the calculation of stresses and SIFs. For the isotropic case, our numerical results are in excellent agreement with those obtained with previously published analytical solutions. For the anisotropic case, our results clearly show that material anisotropy can have a great effect on the stress distribution and the SIFs.

2 BEM FORMULATION FOR 2D CRACKED ANISOTROPIC MEDIA

For a linear elastic medium, we can express, by superposition, the total displacements, stresses, and tractions as follows:

$$u_i^t = u_i^h + u_i^p \quad \sigma_{ij}^t = \sigma_{ij}^h + \sigma_{ij}^p \quad T_i^t = T_i^h + T_i^p \tag{1}$$

where the superscript t, denotes the total solution; h, the homogeneous solution, and p, a particular solution corresponding to the body forces and/or the far-field stresses.

Following the procedure by Pan and Amadei,[23,24] one can show that the internal total displacement solution can be expressed by the following integral:

$$u_i^t(X_p) + -\int_S T_{ij}^*(X_p, X_S)u_j^t(X_S)dS(X_S)$$

$$+ \int_\Gamma T_{ij}^*(X_p, X_{\Gamma+})[u_j^t(X_{\Gamma+}) - u_j^t(X_{\Gamma-})]d\Gamma(X_{\Gamma+})$$

$$= \int_S U_{ij}^*(X_p, X_S)T_j^t(X_S)dS(X_S)$$

$$+ \int_S T_{ij}^*(X_p, X_S)(u_j^p(X_S) - u_i^p(X_p))dS(X_S)$$

$$- \int_S U_{ij}^*(X_p, X_S)T_j^p(X_S)dS(X_S) \tag{2}$$

where dS and dΓ are the line elements on the no-cracked boundary and crack surface, respectively, with the corresponding points being denoted by subscript *s* and Γ (Fig. 1); U_{ij}^* and T_{ij}^* are the Green's displacements and tractions which will be derived in the next section; A point on the positive (or negative) side of a crack is denoted by $X_{\Gamma+}$ (or $X_{\Gamma-}$). In deriving eqn (2), we have assumed that the tractions on the two faces of a crack are equal and opposite.

Let X_p approach a point Y_S on the no-cracked boundary, one arrives at the following boundary integral equation

$$b_{ij}u_j^t(Y_S) + \int_S T_{ij}^*(Y_S, X_S)u_j^t(X_S)dS(X_S)$$

$$+ \int_\Gamma T_{ij}^*(Y_S, X_{\Gamma+})[u_j^t(X_{\Gamma+}) - u_j^t(X_{\Gamma-})]d\Gamma(X_{\Gamma+})$$

$$= \int_S U_{ij}^*(Y_S, X_S)T_j^t(X_S)dS(X_S)$$

$$+ \int_S T_{ij}^*(Y_S, X_S)(u_j^p(X_S) - u_i^p(Y_S))dS(X_S)$$

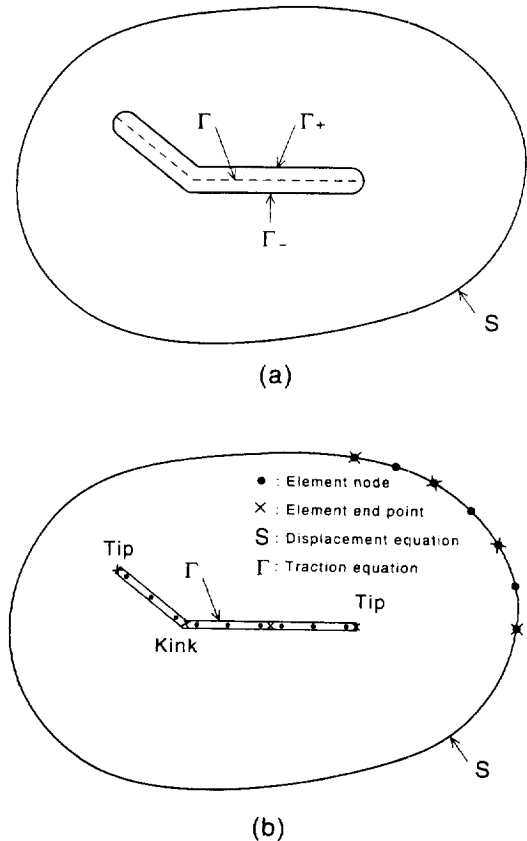$$- \int_S U_{ij}^*(Y_S, X_S)T_j^p(X_S)dS(X_S) \tag{3}$$

Fig. 1. Geometry of a cracked 2D anisotropic domain in (a), and modeling with quadratic boundary elements in (b).

where b_{ij} are coefficients that depend only upon the local geometry of the no-cracked boundary at Y_S.

It is noted that all the terms on the right hand side of eqn (3) have only weak singularities, thus, are integrable. Although the second term on the left-hand side of eqn (3) has a strong singularity, it can be treated by the rigid-body motion method. At the same time, the calculation of b_{ij}, which is geometry dependent, can also be avoided. For problems without cracks, the second integral on the left-hand side of eqn (3) which is related to the crack surface is discarded, and this equation thus reduces to the well-known displacement integral equation. For a cracked domain, however, eqn (3) is not enough for solving the unknowns [25]. For this situation, the traction integral equation [23,26–30] can be adopted and modified. Assume that Y_Γ is a smooth point on the crack, the traction integral equation can be derived as

$$0.5[T_1^l(Y_{\Gamma+}) - T_1^l(Y_{\Gamma-})] + n_m(Y_{\Gamma+})$$

$$\times \int_S c_{lmik} T_{ij,k}^*(Y_{\Gamma+}, X_S) u_j^l(X_S) dS(X_S) + n_m(Y_{\Gamma+})$$

$$\times \int_\Gamma c_{lmik} T_{ij,k}^*(Y_{\Gamma+}, X_{\Gamma+})[u_j^l(X_{\Gamma+}) - u_j^l(X_{\Gamma-})] d\Gamma(X_{\Gamma+})$$

$$= 0.5[T_1^p(Y_{\Gamma+}) - T_1^p(Y_{\Gamma-})] + n_m(Y_{\Gamma+})$$

$$\times \int_S c_{lmik} U_{ij,k}^*(Y_{\Gamma+}, X_S) T_j^l(X_S) dS(X_S) + n_m(Y_{\Gamma+})$$

$$\times \int_S c_{lmik} T_{ij,k}^*(Y_{\Gamma-}, X_S) u_j^p(X_S) dS(X_S) - n_m(Y_{\Gamma+})$$

$$\times \int_S c_{lmik} U_{ij,k}^*(Y_{\Gamma+}, X_S) T_j^p(X_S) dS(X_S) \tag{4}$$

where n_m is the outward normal at the crack surface $Y_{\Gamma+}$ and c_{lmik} is a 4th order stiffness tensor.

It is noted that a formulation similar to eqns (3) and (4) for the homogeneous case (without particular solutions) was presented by Pan and Amadei.[23] This BEM formulation is similar to the dual BEM developed by Portela *et al.*[27], but with the displacement integral equation being collocated on the no-cracked boundary only and the traction integral equation on one side of the crack surface only.

It is noteworthy that in eqns (3) and (4), the effect of the body force of gravity and/or the far-field stresses has been included by superposition of the corresponding particular solutions, which makes the problem very similar to the one associated with the homogeneous equations except that for the body force and/or far-field stress cases, two extra integral terms related to the particular solutions are added to the integral eqns (3) and (4). Thus, the artificial truncation of the infinite domain[31] or transferring of the far-field stress onto the boundary (or opening) of the problem[22] is avoided. It is apparent that the former method introduces errors because of the truncation of the region and increases the size of the problem, the latter may not be suitable for cases where the boundaries or openings have complex shapes.

As mentioned before, for an uncracked domain, only eqn (3) without the crack surface integral term is required. Similarly, for problems containing crack surfaces only, like cracks in an infinite or semi-infinite plane, only eqn (4) is required with the no-crack boundary integral terms being omitted.

The boundary integral eqns (3) and (4) can be discretized and solved numerically for the unknown boundary displacements (or displacement discontinuities on the crack surface) and tractions. In solving these equations, the hypersingular integral term involved in eqn (4) can be handled by an accurate and efficient Gauss quadrature formulae[23,32] while the numerical calculation of the Cauchy type integral in eqn (3) can be avoided with the rigid-body motion method.

Once the boundary problem is solved, eqn (2) can be used to calculate the internal displacements. In order to calculate the internal stresses, we need to first take the derivative of eqn (2) with respect to the internal coordinates X_p. This procedure results in the following equation:

$$u_{i,k}^l(X_p) + \int_S T_{ij,k}^*(X_p, X_S) u_j^l(X_S) dS(X_S)$$

$$+ \int_\Gamma T_{ij,k}^*(X_p, X_{\Gamma+})[u_j^l(X_{\Gamma+}) - u_j^l(X_{\Gamma-})] d\Gamma(X_{\Gamma+})$$

$$= u_{i,k}^p(X_p) + \int_S U_{ij,k}^*(X_p, X_S) T_j^l(X_S) dS(X_S)$$

$$+ \int_S T_{ij,k}^*(X_p, X_S) u_j^p(X_S) dS(X_S)$$

$$- \int_S U_{ij,k}^*(X_p, X_S) T_j^p(X_S) dS(X_S) \tag{5}$$

Once the $u_{i,k}^l$ are obtained, the known constitutive relation can then be used to calculate the internal stresses. It is noted that in the previous eqns (1)–(5), the Green's displacements and stresses (and their derivatives) and the particular solutions of displacements and stresses (tractions) need to be provided. This is discussed in the next two sections.

3 GREEN'S FUNCTIONS IN ANISOTROPIC HALF PLANES

The complex variable function method has been found to be very suitable for the study of 2D anisotropic elastic media[33]. Green's functions for point sources in such an infinite medium were studied by several authors, notably by Eshelby *et al.*[34], Stroh[35], and Lekhnitskii[33]. For an anisotropic half-plane, Green's functions were studied by Suo[36] using the one-complex function method, and by Ting and co-workers[37–39] based on the Stroh tensor method. Here, we follow the one-complex function method introduced by Suo[36].

With three complex analytical functions $f_i(z_i)$, one can, in general, express displacements and stresses as [10,33,36]

$$u_i = 2Re\left[\sum_{j=1}^{3} A_{ij}f_j(z_j)\right]$$

$$\sigma_{2i} = 2Re\left[\sum_{j=1}^{3} L_{ij}f_j'(z_j)\right] \qquad (6)$$

$$\sigma_{1i} = -2Re\left[\sum_{j=1}^{3} L_{ij}\mu_j f_j'(z_j)\right]$$

In these equations, $z_j = x + \mu_j y$ where x and y are Cartesian coordinates; Re denotes the real part of a complex variable or function; and μ_j ($j = 1,2,3$) are three distinct complex roots with positive imaginary part of the following equation:

$$l_1(\mu)l_2(\mu) - l_3^2(\mu) = 0 \qquad (7)$$

where the complex functions l_2, l_3, and l_4 are given in Lekhnitskii.[33] Also in eqn (6), the elements of the complex matrices [L] and [A] depend on the compliance tensor a_{ij} in the (x,y) coordinates. Their expressions can be found in Pan and Amadei,[10] Lekhnitskii,[33] or Suo.[36]

For concentrated forces acting at the source point (x^0, y^0), the complex functions in eqn (6) can be expressed as [36]

$$f_j(z_j) = \sum_{k=1}^{3} \frac{-1}{2\pi}D_{jk}P_k\ln(z_j - z_j^0) \qquad (8)$$

In eqn (8), $z_j^0 = x^0 + \mu_j y^0$, P_k ($k = 1,2,3$) is the magnitude of the point force in the k-direction; and

$$D = A^{-1}(B^{-1} + \overline{B}^{-1})^{-1} \qquad B = iAL^{-1} \qquad (9)$$

where $i = \sqrt{-1}$; overbar means complex conjugate; superscript -1 means matrix inverse.

For a half-plane problem, we let the medium occupy the lower half-plane ($y \leq 0$) and let $y = 0$ correspond to the traction-free surface. To find the complex functions in eqn (6), we assume, as in Suo,[36] the following vector function expression:

$$F^h = F^f + F^c \qquad (10)$$

where the superscripts h and f denote the solutions corresponding to half- and full-plane, respectively, and c is the complementary part of the solutions. The vector function is defined by

$$F(z) = [f_1(z),f_2(z),f_3(z)]^t \qquad (11)$$

While F^f is given by eqn (8), F^c can be solved by substituting F^h into the resultant traction equation and enforcing the traction-free condition at $y = 0$. This procedure involves the analytical continuation of complex functions.[36] The complementary part of the function turns to be very simple and can be written as

$$F^c = -L^{-1}\overline{L}\overline{F}^f \qquad (12)$$

Using eqns (6)–(12), the Green's functions corresponding to the half-plane domain can be derived. For displacements,

these Green's functions are

$$U_{kl}^* = \frac{-1}{\pi}Re$$

$$\times \left\{\sum_{j=1}^{3} A_{lj}[D_{jk}\ln(z_j - z_j^0) - \sum_{i=1}^{3} E_{ji}\overline{D_{ik}}\ln(z_j - \overline{z_i^0})]\right\} \qquad (13)$$

with

$$E = L^{-1}\overline{L} \qquad (14)$$

and for tractions, they are

$$T_{kl}^* = \frac{1}{\pi}Re\left\{\sum_{j=1}^{3} L_{lj}[\frac{\mu_j n_x - n_y}{z_j - z_j^0}D_{jk} - \sum_{i=1}^{3} E_{ji}\frac{\mu_j n_x - n_y}{z_j - \overline{z_i^0}}\overline{D_{ik}})]\right\} \qquad (15)$$

In eqn (15), n_x and n_y are the outward normal components of the field point z_j. For the calculation of internal stresses (eqn (5)), we need the derivative of the above Green's functions with respect to the source point z_i^0. The derivatives of the Green's displacement and traction yield

$$U_{kl,x^0}^* = \frac{1}{\pi}Re\left\{\sum_{j=1}^{3} A_{lj}[D_{jk}\frac{1}{z_j - z_j^0} - \sum_{i=1}^{3} E_{ji}\overline{D_{ik}}\frac{1}{z_j - \overline{z_i^0}}]\right\}$$

$$U_{kl,y^0}^* = \frac{1}{\pi}Re\left\{\sum_{j=1}^{3} A_{lj}[D_{jk}\frac{\mu_j}{z_j - z_j^0} - \sum_{i=1}^{3} E_{ji}\overline{D_{ik}}\frac{\overline{\mu_i}}{z_j - \overline{z_i^0}}]\right\} \qquad (16)$$

and

$$T_{kl,x^0}^* = \frac{1}{\pi}Re\left\{\sum_{j=1}^{3} L_{lj}\left[\frac{\mu_j n_x - n_y}{(z_j - z_j^0)^2}D_{jk}\right.\right.$$

$$\left.- \sum_{i=1}^{3} E_{ji}\frac{\mu_j n_x - n_y}{(z_j - \overline{z_i^0})^2}\overline{D_{ik}}\right]\right\}$$

$$T_{kl,y^0}^* = \frac{1}{\pi}Re\left\{\sum_{j=1}^{3} L_{lj}\left[\frac{(\mu_j n_x - n_y)\mu_j}{(z_j - z_j^0)^2}D_{jk}\right.\right.$$

$$\left.- \sum_{i=1}^{3} E_{ji}\frac{(\mu_j n_x - n_y)\overline{\mu_i}}{(z_j - \overline{z_i^0})^2}\overline{D_{ik}}\right]\right\} \qquad (17)$$

It is noteworthy that the Green's functions in eqns (13)–(17) can be used to solve both plane stress and plane strain problems[23] in both anisotropic half- and full-planes (for the full-plane case, the Green's functions are those given by the first summation terms in eqns (13), (15)–(17)[23]). Although the isotropic solution cannot be analytically reduced from these Green's functions, one can numerically approximate it by selecting a very weak anisotropic (or nearly isotropic) medium.[23,40]

4 PARTICULAR SOLUTIONS OF GRAVITY AND FAR-FIELD STRESSES

As mentioned in the previous section, if the particular solutions corresponding to the body force of gravity and

far-field stresses can be derived in exact closed-form, the BEM formulation presented in this paper can then be applied and implemented.[23] For the body force of gravity, the exact closed-form solutions can be obtained in a similar way as for the corresponding half-space.[41] Assuming that the gravity has the components g_x and g_y in the x- and y-directions, respectively, the particular solution for the displacement components can be found as:

$$u_x^p = a_1 \rho g_x x^2 + b_1 \rho g_y y^2 \quad u_y^p = a_2 \rho g_x x^2 + b_2 \rho g_y y^2 \quad (18)$$

where coefficients a_i and b_i depend on the elastic stiffness and their expressions are given in Appendix A.

Similarly, the particular stresses can be expressed as

$$\begin{bmatrix} \sigma_{11}^p \\ \sigma_{22}^p \\ \sigma_{23}^p \\ \sigma_{13}^p \\ \sigma_{12}^p \end{bmatrix} = \begin{bmatrix} d_{11} & d_{12} \\ d_{21} & d_{22} \\ d_{41} & d_{42} \\ d_{51} & d_{52} \\ d_{61} & d_{62} \end{bmatrix} \begin{bmatrix} \rho g_x x \\ \rho g_y y \end{bmatrix} \quad (19)$$

Again, d_{ij} depend on the elastic coefficients and their expressions are given in Appendix A.

For a half-plane under a far-field stress T in the x-direction, the particular stress solution is simply

$$\sigma_{xx}^p = T; \sigma_{ij}^p = 0 \text{ if } (i,j) \neq (x,x) \quad (20)$$

The corresponding particular displacements can be assumed as

$$u_x^p = 2a_1 Tx \quad u_y^p = 2a_2 Tx \quad (21)$$

where a_1 and a_2 are coefficients given in Appendix A. It should be emphasized that in most opening related problems, we are only interested in the opening-induced

displacements (or the displacements relative to those before the opening). In these circumstances, the particular displacement solutions related to the body force of gravity and the far-field stresses can be set to zero.

5 NUMERICAL EXAMPLES

The aforementioned Green's functions and the particular solutions were incorporated into the boundary integral eqns (2)–(5), and the results were programmed. In this section, several numerical examples are presented to verify the formulation and the program, and also to show the efficiency of the present BEM formulation for anisotropic and elastic half-planes. For the isotropic case, the Young's modulus was assumed as $E = 4 (10^4$ MPa) and the Poisson's ratio as $\nu = 0.25$. In the anisotropic case, the elastic constants were taken from Lekhniskii[33] which corresponds to a plywood material modeled as transversely isotropic: $E = 0.6 (10^4$ MPa), $E' = 1.2 (10^4$ MPa), $\nu = 0.25$, $\nu' = 0.071$, $G' = 0.07 (10^4$ MPa). Here E and E' are Young's moduli in the plane of transverse isotropy and in the direction normal to it, respectively; ν and ν' are Poisson's ratios characterizing the lateral strain response in the plane of transverse isotropy to a stress acting parallel and normal to it, respectively; and G' is the shear modulus in planes normal to the plane of transverse isotropy. Also, for the numerical examples related to the anisotropic case, ψ is an angle such that $\psi = 0°$ denotes the case where the plane of transverse isotropy contains the x-axis, and $\psi = 90°$ denotes the case where the plane of transverse isotropy contains the y-axis.
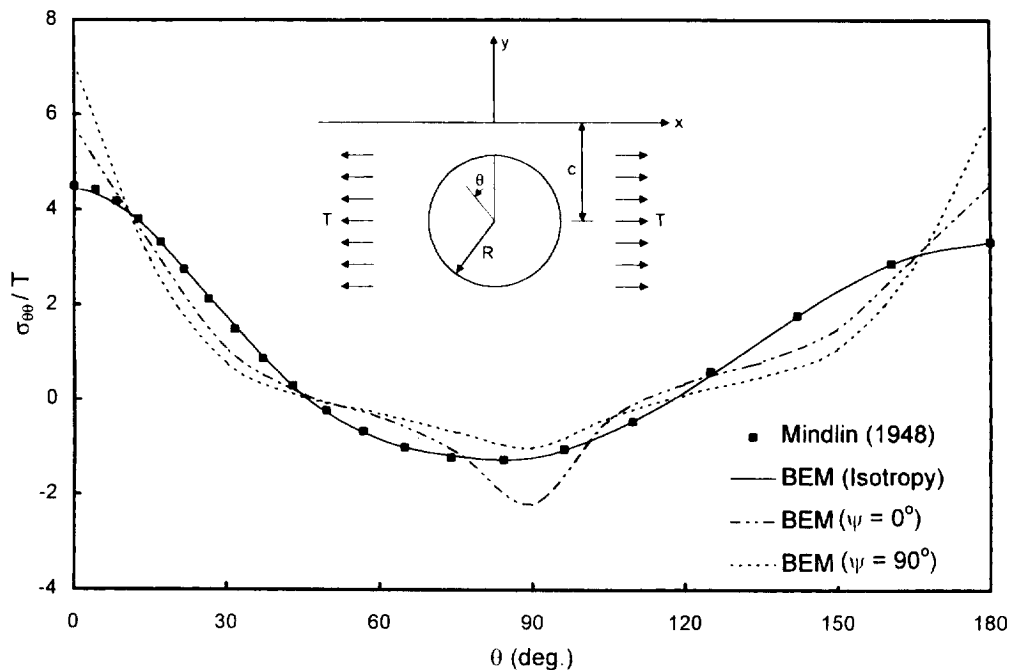

Fig. 2. Variation of the normalized hoop stress $\sigma_{\theta\theta}/T$ along the wall of a circular opening, under a far-field stress of magnitude T $(c/R = 1.54)$.
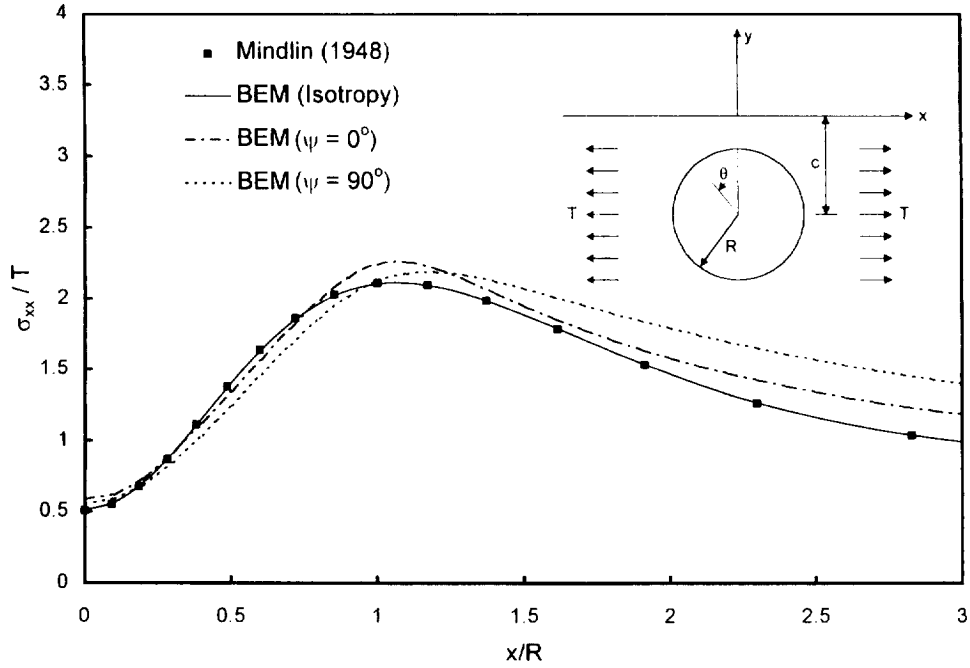
Fig. 3. Variation of the normalized horizontal stress σ_{xx}/T along the flat surface ($y = 0$), under a far-field stress of magnitude T ($c/R = 1.54$).

5.1 Example 1

This example corresponds to an internal circular opening under a far-field stress T in the x (or horizontal) direction or gravity g in the y (or vertical) direction (Figs 2–5). While the far-field stress case is under a plane stress condition (this also applies to the following examples), a plane strain condition is assumed for the gravity case. The opening has

a radius R and its center is located at a depth c such that $c/R = 1.54$. Twelve quadratic elements with a total of 24 nodes were used to discretize the whole boundary of the opening. Stresses were determined along the wall of the opening and along the surface of the half-plane ($y = 0$) for the isotropic case and the anisotropic case when $\psi = 0°$ (horizontal transverse isotropy) and $\psi = 90°$ (vertical transverse isotropy). Figures 2 and 3 show, respectively,
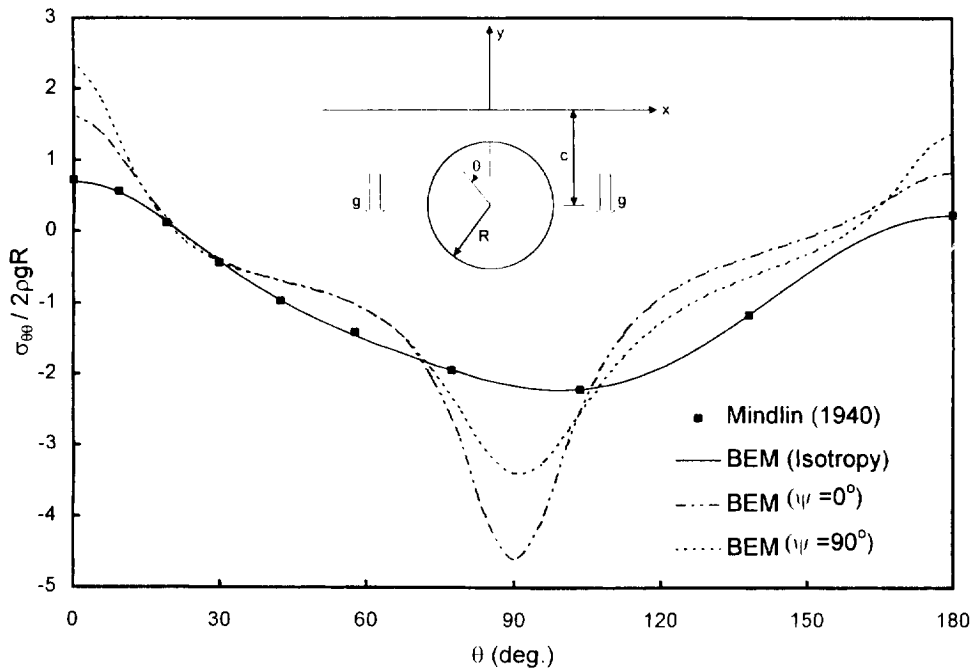

Fig. 4. Variation of the normalized hoop stress $\sigma_{\theta\theta}/2\rho gR$ along a circular opening, under the body force of gravity ($c/R = 1.54$).
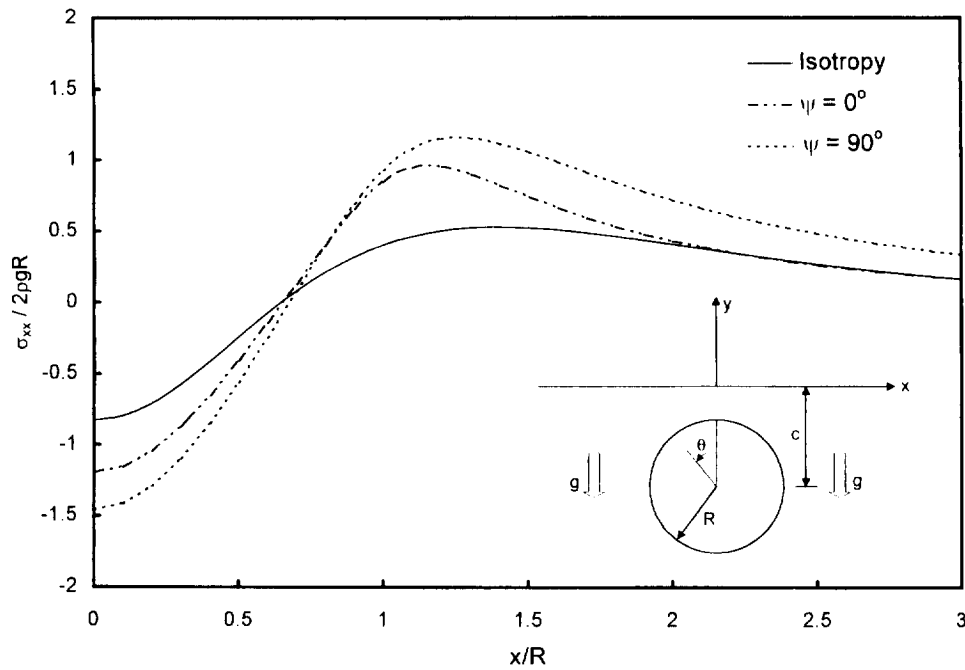
Fig. 5. Variation of the normalized horizontal stress $\sigma_{xx}/2\rho g R$ along the flat surface ($y = 0$), under the body force of gravity ($c/R = 1.54$).

the variation of the normalized hoop stress $\sigma_{\theta\theta}/T$ along the wall of the opening and the variation of the normalized horizontal stress σ_{xx}/T along the flat surface ($y = 0$) when T is acting only. Figs 4 and 5 are the corresponding stress variations under gravity only. For the isotropic case, the stresses obtained with our BEM program were compared with those determined analytically by Mindlin[1,2] using a bipolar co-ordinate system. Figs 2–4 indicate that for the isotropic case, our numerical solutions are in excellent agreement with Mindlin's solutions. These figures also show that anisotropy has an effect on the stress magnitude and distribution. For instance, in Figs 2 and 4, vertical anisotropy ($\psi = 90°$) creates more tension at $\theta = 0°$ and $180°$ than the isotropic case. In Fig. 4, more compression is induced at $\theta = 90°$ when the medium is anisotropic. For points located along the flat surface ($y = 0$), and under gravity, Fig. 5 shows that anisotropy induces more compression in the horizontal direction above the opening and more tension away from the opening. Under T only (Fig. 3), the effect of anisotropy on the magnitude of σ_{xx} becomes apparent for $x/R > 1.5$. For instance, at $x/R = 3$, the horizontal stress still differs significantly from the far-field stress T (Fig. 3, e.g. $\sigma_{xx}/T = 1.3961$ for the anisotropic case $\psi = 90°$).

Table 1. Normalized hoop stress $\sigma_{\theta\theta}/T$

	BEM ($e/R = 0.5$)			Chen [42]
	$\psi = 0°$	$\psi = 90°$	Isotropy	Isotropy
A	3.878	4.970	2.900	2.84
B	−0.300	−0.236	−0.134	−0.11
C	5.011	6.100	3.993	3.81
D	−1.587	−0.756	−0.930	−0.90

5.2 Example 2

Our BEM formulation is numerical, it can be used to analyze the stress distribution around an opening of any shape or around multiple openings located site by site. Fig. 6 shows a half-plane under a horizontal far-field stress T, which is weakened by two circular openings of radius R separated by a distance e such that $e/R = 0.5$. For the isotropic case, Chen[42] solved the stresses using an approximate method, i.e., the eigenfunction expansion and variational methods. In our BEM modeling, 24 quadratic elements with a total of 48 nodes for both circles were used to discretize the boundary. The normalized hoop stress concentrations at points A, B, C and D on the boundary (Fig. 6) are listed in Table 1 for both the anisotropic and isotropic cases. The variation of the normalized horizontal stress σ_{xx}/T along the flat surface ($y = 0$) is plotted in Fig. 6. As we can see from Table 1, for the isotropic case, the stresses from our BEM modeling are in good agreement with those determined by Chen[42]. For the anisotropic case, one can observe from Table 1 and Fig. 6 the effect of the material anisotropy on the stress distribution along the circular boundary and the flat surface. For instance, at both points A and C on the opening, the hoop stresses for the anisotropic case are much greater than those for the isotropic case. Also, for points along the flat

Table 2. Stress concentrations at point A

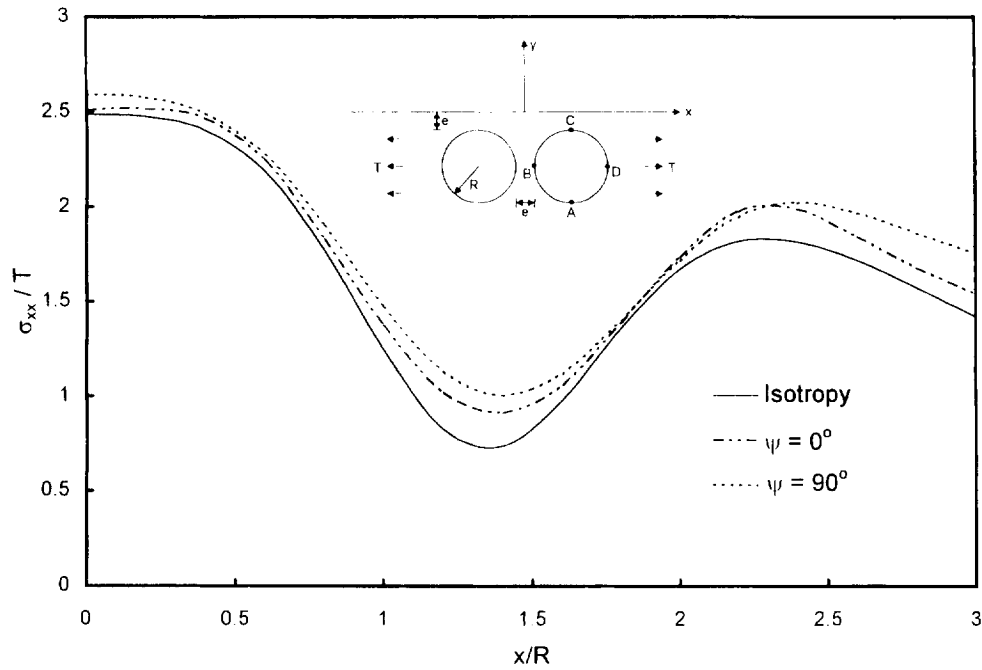|	BEM	Ling [3]
Isotropy	3.065	3.065
$\psi = 0°$	4.197	-
$\psi = 90°$	5.542	-

Fig. 6. Variation of the normalized horizontal stress σ_{xx}/T along the flat surface ($y = 0$), under a far-field stress of magnitude T ($e/R = 0.5$).

surface ($y = 0$), we observed that the horizontal stresses for both anisotropic cases are greater than that for the isotropic case

5.3 Example 3

As a third example consider a half-circular opening ($a = R$) under a far-field stress T in the horizontal direction (Figs 7 and 8). For this case, 10 quadratic elements with a total of 21

nodes are used to discretize the boundary. The normalized stress concentrations at the bottom point A are given in Table 2 along with the result obtained with the analytical solution by Ling[3] using a bipolar coordinate system. Table 2 indicates that for the isotropic case, our numerical result is exactly the same as the analytical solution. Variations of the normalized stresses along the circular and horizontal surfaces are shown, respectively, in Figs 7 and 8. Again, we like to emphasize that the effect of anisotropy is apparent,
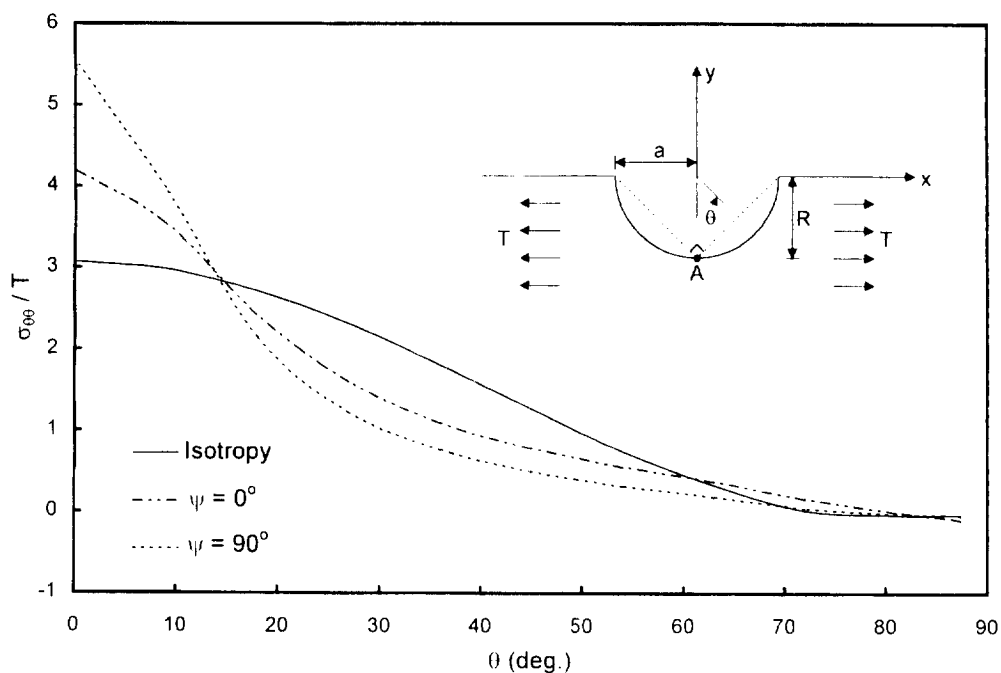

Fig. 7. Variation of the normalized hoop stress $\sigma_{\theta\theta}/T$ along the half circle, under a far-field stress of magnitude T ($a/R = 1$).
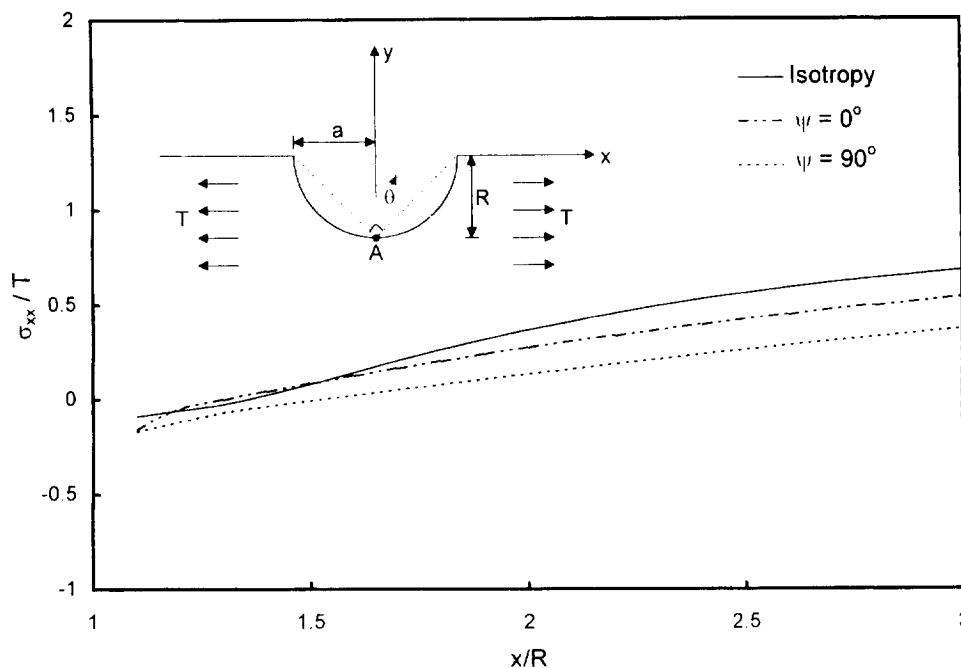
Fig. 8. Variation of the normalized horizontal stress σ_{xx}/T along the flat surface ($y = 0$), under a far-field stress of magnitude T ($a/R = 1$).

and must be considered in the strength estimation of defected materials and in predicting the stress distribution of valley walls in layered media.

5.4 Example 4

As a final example consider an inclined crack under a far-field horizontal stress of magnitude T (Fig. 9). The crack length is a and it is inclined β degrees to the horizontal direction. The crack is discretized by 10 discontinuous quadratic elements with a total of 30 crack nodes. Different from the previous examples where only the displacement integral eqn (3) is required, here only the traction boundary integral eqn (4) is needed. Once the boundary value problem is solved, the method presented in Pan and Amadei[23] and Sollero and Aliabadi[29] can then be employed to calculate the SIFs. The results, normalized with respect to $K_0 = T\sqrt{(\pi a)}$, for $\beta = 30°$, $45°$, and $90°$, are shown in Table 3 and 4, respectively, for the isotropic and anisotropic cases. As can be seen from Table 3, the SIFs determined with our BEM program are very close to those obtained by Noda and Matsuo[43] using the discontinuously distributed dislocation method. Table 4 shows the corresponding SIFs when the material is anisotropic. Comparison

of Tables 3 and 4 shows the effect of the material anisotropy on the SIFs.

6 CONCLUSION

We have presented a general 2-D BEM formulation for the analysis of problems related to anisotropic and cracked half-planes. The corresponding program can be used for the gravity and/or far-field stress cases, for problems with or without boundary tractions on the flat surface of the half-plane or along the surface of openings. For the isotropic case, we compared our results with existing analytical solutions, and found that even with relatively coarse discretizations, very accurate results could be obtained. This is because the Green's functions corresponding to the half-plane were included and no discretization along the flat surface of the half-plane is necessary. The results for the anisotropic case have clearly shown the effect of anisotropy on the stress distribution and the SIFs.

The current BEM program can find applications in material sciences to study the effect of defects' size and shape, and of material anisotropy, on the stress distribution, the SIF, and on the stability of stressed surfaces.[4,7,9,44] It can

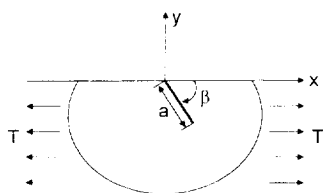**Fig. 9.** Geometry of an inclined edge crack under a far-field stress.

Table 3. Normalized SIFs for the isotropic case

β (degrees)	BEM		Noda and Matsuo [43]	
	K_{I}/K_0	K_{II}/K_0	K_{I}/K_0	K_{II}/K_0
90	1.1217	0	1.1215	0
45	0.7093	0.3578	0.7049	0.3645
30	0.4696	0.3283	0.4625	0.3362

Table 4. Normalized SIFs for the anisotropic case by the BEM

β (degrees)	$\psi = 0°$		$\psi = 90°$	
	K_I/K_0	K_II/K_0	K_I/K_0	K_II/K_0
90	1.0605	0	1.0675	0
45	0.7608	0.3837	0.7297	0.5004
30	0.4116	0.3217	0.3276	0.3477

also find applications in excavation-related engineering to study problems when gravity and tectonic stresses co-exist.

Extension to the crack-growth simulation is now under investigation. Completion of such work could be used to predict the initiation and simulate the evolution of defects or flaws in advanced materials like heteroepitaxial thin films,[4,9] or to model fatigue crack growth,[45] and to study rock slope stability, borehole breakout, and rock fracture propagation. It can also help in the performance assessment of tunnels[46] and in in-situ stress estimation in complex environment.[47]

ACKNOWLEDGEMENTS

REFERENCES

1. Mindlin, R.D. Stress distribution around a tunnel. *Transactions of the American Society of Civil Engineers*, 1940, **105**, 1117–1153.

2. Mindlin, R. D. Stress distribution around a hole near the edge of a plate under tension. In *Proc. of The Society for Experimental Stress Analysis*. 1948, Vol. 5, 56-68.

3. Ling, C.B. On the stresses in a notched plate under tension. *J. Math. Phys.*, 1947, **26**, 284–289.

4. Srolovitz, D.J. On the stability of surfaces of stressed solids. *Acta Metal.*, 1989, **37**, 621–625.

5. Liao, J.J., Savage, W.Z. and Amadei, B. Gravitational stresses in anisotropic ridges and valleys with small slopes. *J. Geophys. Res.*, 1992, **97**, 3325–3336.

6. Gao, H. Stress concentration at slightly undulating surfaces. *J. Mech. Phys. Solids*, 1991, **39**, 443–458.

7. Gao, H. Morphological instabilities along surfaces of anisotropic solids. In *Modern Theory of Anisotropic Elasticity and Applications*, ed. J. J. Wu, T. C. T. Ting & D. M. Barnett, SIAM, Philadelphia, 1991, pp. 139-150.

8. Savage, W.Z. and Swolfs, H.S. Tectonic and gravitational stress in long symmetric ridges and valleys. *J. Geophys. Res.*, 1986, **91**, 3677–3685.

9. Chiu, C. and Gao, H. Stress singularities along a cycloid rough surface. *Int. J. Solids Structures*, 1993, **30**, 2983–3012.

10. Pan, E. and Amadei, B. Stress concentration at irregular surfaces of anisotropic half-spaces. *Acta Mech.*, 1995, **113**, 119–135.

11. Pan, E., Amadei, B. and Savage, W.Z. Gravitational and tectonic stresses in anisotropic rock with irregular topography. *Int. J. Rock. Mech. Min. Sci. and Geomech. Abstr.*, 1995, **32**, 201–214.

12. Zienkiewicz, O.C., Cheung, Y.K. and Stagg, K.G. Stresses in anisotropic media with particular reference to problems of rock mechanics. *J. Strain Analysis*, 1966, **1**, 172–182.

13. Barla, G. Stresses around a single underground opening near a tension-free surface. *Int. J. Rock Mech. Min. Sci. and Geomech. Abstr.*, 1972, **9**, 103-126.

14. Soliman, E., Duddeck, H. and Ahrens, H. Two- and three-dimensional analysis of closely spaced double-tube tunnels. *Tunelling and Undergound Space Technology*, 1993, **8**, 13–18.

15. Eissa, E. A. Stress analysis of underground excavations in isotropic and stratified rock using the boundary element method. PhD thesis, Imperial College of Science and Technology, London, 1980.

16. Fainstein, G., Sidi, A., Israeli, M. & Tsur-Lavie, Y. Application of boundary integral equations to the solution of stresses around a shallow circular hole. In *28th US Symposium, on Rock Mechanics*. 1987, pp. 745-754.

17. Carter, J.P. and Alehossein, H. Analysis of tunnel distortion due to an open excavation in jointed rock. *Comp. Geotech.*, 1990, **9**, 209–231.

18. Xiao, B. and Carter, J.P. Boundary element analysis of anisotropic rock masses. *Eng. Analy. Boundary Elements*, 1993, **11**, 293–303.

19. Beer, G. and Poulsen, B.A. Analysis of infinitely long excavations using finite and boundary elements. *Int. J. Numer. Anal. Meth. Geomech.*, 1994, **18**, 417–426.

20. Telles, J.C.F. and Brebbia, C.A. Boundary element solution for half-plane problems. *Int. J. Solids Structures*, 1981, **17**, 1149–1158.

21. Meek, J.L. and Dai, C. Boundary element modeling: Near surface excavations. *Computer Meth. Appl. Mech. Eng.*, 1993, **102**, 15–27.

22. Dumir, P.C. and Mehta, A.K. Boundary element solution for elastic orthotropic half-plane problems. *Computers and structures*, 1987, **26**, 431–438.

23. Pan, E. and Amadei, B. Fracture mechanics analysis of cracked 2-D anisotropic media with a new formulation of the boundary element method. *Int. J. Fracture*, 1996, **77**, 161–174.

24. Pan, E. and Amadei, B. A 3-D boundary element formulation of anisotropic elasticity with gravity. *Appl. Math. Modelling*, 1996, **20**, 114–120.

25. Aliabadi, M. H. and Rooke, D. P. *Numerical Fracture Mechanics*. Computational Mechanics Publications. 1991.

26. Hong, H.K. and Chen, J.T. Derivations of integral equations of elasticity. *J. Eng. Mech.*, 1988, **114**, 1028–1044.

27. Portela, A., Aliabadi, M.H. and Rooke, D.P. The dual boundary element method: Effective implementation for crack problems. *Int. J. Numer. Meth. Eng.*, 1992, **33**, 1269–1287.

28. Guimaraes, S. and Telles, J.C.F. On the hyper-singular boundary-element formulation for fracture-mechanics applications. *Eng. Analy. Boundary elements*, 1994, **13**, 353–363.

29. Sollero, P. and Aliabadi, M.H. Anisotropic analysis of cracks in composite laminates using the dual boundary element method. *Computers and Structures*, 1995, **31**, 229–234.

30. Aliabadi, M.H. Boundary element formulations in fracture mechanics. *Appl. Mech. Rev.*, 1997, **50**, 83–96.

31. Lee, J.S. Boundary element method for electroelastic interaction in piezoceramics. *Eng. Anal. Bound. Elements*, 1995, **15**, 321–328.

32. Tsamasphyros, G. and Dimou, G. Gauss quadrature rules for finite part integrals. *Int. J. Numer. Methods Eng.*, 1990, **30**, 13–26.

33. Lekhnitskii, S. G. *Theory of Elasticity of an Anisotropic Body*. Holden Day, San Francisco, 1963.

34. Eshelby, J.D., Read, W.T. and Shockley, W. Anisotropic elasticity with applications to dislocations theory. *Acta Metal.*, 1953, **1**, 251–259.

35. Stroh, A.N. Dislocations and cracks in anisotropic elasticity. *Philos. Mag.*, 1958, **7**, 625–646.

36. Suo, Z. Singularities, interfaces and cracks in dissimilar anisotropic media. *Proc. R. Soc. Lond.*, 1990, **A427**, 331–358.

37. Ting, T.C.T. Image singularities of Green's functions for anisotropic elastic half-spaces and bimaterials. *Q. J. Mech. Appl. Math.*, 1992, **45**, 119–139.

38. Ting, T.C.T. and Barnett, D.M. Image force on line dislocations in anisotropic elastic half-spaces with a fixed boundary. *Int. J. Solids Structures*, 1993, **30**, 313–323.

39. Wei, L. and Ting, T.C.T. Explicit expressions of the Barnett-Lothe tensors for anisotropic materials. *J. Elasticity*, 1994, **36**, 67–83.

40. Sollero, P., Aliabadi, M.H. and Rooke, D.P. Anisotropic analysis of cracks emanating from circular holes in composite laminates using the boundary element method. *Eng. Fracture. Mech.*, 1994, **49**, 213–224.

41. Amadei, B. and Pan, E. Gravitational stresses in anisotropic rock masses with inclined strata *Int. J. Rock Mech. Min. Sci. and Geomech. Abstr.*, 1992, **29**, 225–236.

42. Chen, Y.Z. Multiple circular hole problem for an elastic half-plane. *Computers and Structures*, 1994, **52**, 1277–1281.

43. Noda, N.A. and Matsuo, T. Numerical solutions of singular integral equations having Cauchy-type singular kernel by means of expansion method. *Int. J. Fracture*, 1993, **63**, 229–245.

44. Savin, G. N. *Stress Concentration Around Holes*. Pergamon Press, New York, 1961.

45. Portela, A., Aliabadi, M.H. and Rooke, D.P. Dual boundary element incremental analysis of crack propagation. *Computers and Structures*, 1993, **46**, 237–247.

46. Wong, R.C.K. and Kaiser, P.K. Performance assessment of tunnels in cohersionless soils. *J. Geotechnical Eng.*, 1991, **117**, 1880–1901.

47. Haimson, B. C., Lee, C. F. & Huang, J. H. S. High horizontal stresses at Niagara Falls, their measurement, and the design of a new hydroelectric plant. In *Proc. Int. Symp. Rock Stresses and Rock Stress Measurements*, 1986, pp. 615-624.

APPENDIX A

In the particular solutions of displacements caused by the body force of gravity (eqn (18)) and by a far-field stress in the x-direction (eqn (21)), the coefficients are

$$a_1 = 0.5(c_{55}c_{66} - c_{56}c_{56})/\Delta_1 \quad a_2 = 0.5(c_{15}c_{56} - c_{55}c_{16})/\Delta_1 \tag{A1}$$

$$b_1 = 0.5(c_{24}c_{46} - c_{26}c_{44})/\Delta_2 \quad b_2 = 0.5(c_{44}c_{66} - c_{46}c_{46})/\Delta_2 \tag{A2}$$

where

$$\Delta_1 = c_{11}c_{55}c_{66} + 2c_{16}c_{15}c_{56} - c_{55}c_{16}^2 - c_{11}c_{56}^2 - c_{66}c_{15}^2$$
$$\Delta_2 = c_{22}c_{44}c_{66} + 2c_{26}c_{24}c_{46} - c_{44}c_{26}^2 - c_{22}c_{46}^2 - c_{66}c_{24}^2 \tag{A3}$$

and c_{ij} are the elastic stiffness coefficients.

Similarly, in the particular solution of stress caused by the body force of gravity (eqn (19)), the coefficients are

$$d_{11} = 1 \quad d_{21} = 2(a_1c_{12} + a_2c_{26})$$
$$d_{41} = 2(a_1c_{14} + a_2c_{46}) \quad d_{51} = 0 \quad d_{61} = 0 \tag{A4}$$

$$d_{12} = 2(b_2c_{12} + b_1c_{16}) \quad d_{22} = 1 \quad d_{42} = 0$$
$$d_{52} = 2(b_2c_{25} + b_1c_{56}) \quad d_{62} = 0 \tag{A5}$$